

Connecting wave functions at a three-leg junction of one-dimensional channels

Khee-Kyun Voo,¹ Shu-Chuan Chen,¹ Chi-Shung Tang,² and Chon-Saar Chu¹

¹Department of Electrophysics, National Chiao Tung University, Hsinchu 30010, Taiwan, Republic of China

²Physics Division, National Center for Theoretical Sciences, Hsinchu 30013, Taiwan, Republic of China

(Dated: April 14, 2024)

We propose a scheme to connect the wave functions on different one-dimensional branches of a three-leg junction (Y-junction). Our scheme differs from that due to Gri th [Trans. Faraday Soc. 49, 345 (1953)] in the respect that ours can model the difference in the widths of the quasi-one-dimensional channels in different systems. We test our scheme by comparing results from a doubly-connected one-dimensional system and a related quasi-one-dimensional system, and we find a good agreement. Therefore our scheme may be useful in the construction of one-dimensional effective theories out of (multiply-connected) quasi-one-dimensional systems.

PACS numbers: 73.23.Ad, 73.63.Nm, 73.21.Hb, 02.10.Ox

I. INTRODUCTION

For a system which comprises quasi-one-dimensional (Q1D) channels, when only the low-energy regime at near the first subband bottom is considered, it can usually be modeled by a one-dimensional (1D) system. When the system is multiply-connected and consists of multi-leg junctions, the wave functions on the branches are usually connected at the junctions by the Gri th scheme,^{1,2,3,4} the Shapiro scheme,^{5,6,7} or schemes alike. Since such formulations greatly reduce the calculational effort of complicated multiply-connected mesoscopic systems, they have been used widely in the literature. For example, see Refs. 8,9,10,11,12,13,14,15,16,17,18,19 and the references therein. However, arguments which lead to these connecting schemes are kinematical,^{1,2,3,4,5,6,7} and it is not clear what kind of junction in practice they describe. Moreover, a comparison between the results of these schemes and that of the exact calculation of Q1D systems has never been done. It is the purpose of this paper to make a comparison between the Gri th result, the Q1D result, and the result due to a scheme we propose in this paper. We find that for clean junctions of Q1D channels, the Gri th result is not even qualitatively in accord with the exact result. The scheme we derive gives a result that compares much better with the exact result.

At a N-leg junction of 1D channels, the wave function continuity condition is a requirement that must be respected. Besides, the Gri th scheme^{1,2,3,4} demands that the sum of the derivatives of the wave functions on the different branches at the junction is zero, i.e.,

$$\sum_{i=1}^N \frac{\partial \psi_i}{\partial x_i} = 0; \quad (1)$$

where the directions of the coordinates are defined either diverging from or converging to the junction. This is the simplest way to impose the unitarity condition of no net current flows into the junction, i.e., $\sum_{i=1}^N \text{Re}(\psi_i \partial \psi_i / \partial x_i) = 0$. When there is a magnetic

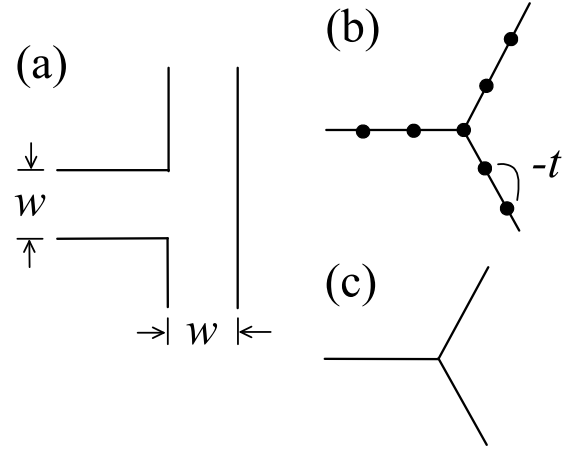


FIG. 1: (a) The original Y-junction of Q1D channels considered in this paper, (b) the reformulated Y-junction of tight-binding channels, and (c) the effective Y-junction of 1D channels associated with the Gri th or our connection scheme.

field, the requirement is rephrased as the sum of the covariant derivatives is zero, i.e., $\sum_{i=1}^N (\partial \psi_i / \partial x_i - ie A_i^k) \psi_i = 0$, where A_i^k is the component of the vector potential parallel to branch i at the junction. On the other hand, the Shapiro scheme^{5,6,7} directly demands that the scattering matrix connecting the in-going and out-going waves at the junction be unitary, and a general matrix with free parameters is written down. When the spin degree of freedom is considered, these schemes are straightforwardly applied to each spin channel.^{15,16,17,18,19} These schemes and the likes have been taken for granted and used widely in the literature.

II. FORMULATIONS AND MODELS

We approach the problem from another point of view. For a Q1D system with equal-width channels (the "width" is an ill-defined quantity in snaking channels but nevertheless we may talk about it when the curvatures

are small enough), we may approximate a three-leg junction (Y-junction) and its branches [e.g., see Fig. 1 (a)] by a tight-binding (TB) model as shown in Fig. 1 (b).²⁰

The tight-binding model is described by a second quantised Hamiltonian

$$H = \sum_{i,j} c_i^\dagger h_{ij} c_j; \quad (2)$$

where c_i is the annihilation operator of a spinless particle on site i , and h_{ij} is a matrix element which is complex in general. The element h_{ij} is called a hopping when $i \neq j$, and an onsite potential when $i = j$. Defining a basis set $\{|\mathbf{j}\rangle\}$ by $|\mathbf{j}\rangle = \sum_i c_i^\dagger |\mathbf{j}\rangle$, where $|\mathbf{j}\rangle$ is the no-particle state, one can write the time-independent Schrödinger equation $H|\mathbf{j}\rangle = E|\mathbf{j}\rangle$, where E is the energy of the particle, into the form

$$\sum_j (h_{ij} - E \delta_{ij}) \psi_j = 0; \quad (3)$$

where $\psi_j = \langle \mathbf{j} | \mathbf{j} \rangle$ is the TB wave function at site j . We define that the hopping exists only between nearest-neighbor sites, and be denoted by t . The onsite potential at site i is denoted by $V_i + t$.

The magnitude of the hopping t is obtained by the following argument. Let a Q1D channel be approximated by a finite-difference square grid, with three grid-points across the channel, one at the center and each edge. Then the distance between the grid-points will be $w=2$, where w is the width of the channel, and the hopping in the finite-difference time-independent Schrödinger equation²¹ will be $t = -\frac{\hbar^2}{2m} \frac{d^2}{dx^2} \psi(x) = [V(x) - E] \psi(x) = 0$. We will assume the same hopping in our TB formulation.

Away from the junction, the TB time-independent Schrödinger equation reads²¹

$$t(\psi_{i+1} - \psi_i) + t(\psi_i - \psi_{i-1}) + (V_i - E) \psi_i = 0; \quad (4)$$

where E is the energy. In the long-wavelength limit it reduces, as it should, to the 1D second order differential time-independent Schrödinger equation, $[-\frac{\hbar^2}{2m} \frac{d^2}{dx^2} \psi(x) + [V(x) - E] \psi(x) = 0$.

At a Y-junction, the TB time-independent Schrödinger equation reads,

$$(\psi_1 - \psi_0) + (\psi_2 - \psi_0) + (\psi_3 - \psi_0) + \frac{E - V_0 + t}{t} \psi_0 = 0; \quad (5)$$

where the subscript "0" denotes the site at the junction, and "1", "2", and "3" denote the sites on the branches nearest to the site at the junction [i.e., in Eq. (3), take $i = 0$, and $j = 0; 1; 2$, and 3]. It is seen that the Grieth scheme formulated in Eq. (1) is recovered only when $E - V_0 + t = 0$ at the junction. It is reasonable to set $E = 0$ here since we are considering energies at near the band-bottom and $E \ll t$. But one still requires $V_0 = t$ to send the last term in Eq. (5) to zero. In other words, the Grieth connection scheme^{1,2,3,4} actually describes a

Y-junction of Q1D channels with a repulsive potential with a strength of the order of t . Whereas in this paper we propose a connection scheme in the long-wavelength limit for a clean Y-junction [i.e., $V_0 = 0$ in Eq. (5)] of Q1D channels. At a Y-junction of 1D channels [see Fig. 1 (c)], we propose

$$\sum_{i=1}^3 \frac{\partial \psi_i}{\partial x_i} + \frac{2}{w} \psi_0 = 0; \quad (6)$$

where the directions of the coordinates are defined to be diverging from the junction. If Eq. (6) is reached by dividing Eq. (5) by $w=2$ and letting $w \rightarrow 0$ (remember that $E=t$ and $V_0=t$ have been set to zero), the factor will be equal to 1. Adopting $\hbar = 1$ indeed results in a good enough qualitative comparison with the Q1D result. But we will see that choosing $\hbar = 1.9$ may bring the 1D and Q1D results to a semi-quantitative agreement, which means that the term \hbar has been underestimated. The TB argument serves to bring out the $1/w$ dependence of the term, and the scaling of w will be discussed using concrete examples. The effect of the channel width is hence included, in contrast to the Grieth scheme (the case of $w = 0$). The $1/w$ dependence results in an effect that is more prominent at smaller channel widths, and this understanding may also help to relate studies on the quantum graph theory^{4,7} to the practical experiments. The case of a general N -leg junction can also be worked out likewise.

In this paper we compare the Grieth and our schemes with the exact Q1D calculation in a chosen type of system. We calculate the transmission probability for a 1D ring connected to two leads [see Fig. 2 (a)], which is the simplest multiply-connected 1D system, using the Grieth and our connection schemes at the Y-junctions. In addition, we also calculate the transmission probability for a similar system, an annulus connected to two Q1D leads [see Fig. 2 (b)], using the exact mode-matching method. The two three-leg junctions in Fig. 2 (b) resemble the one in Fig. 1 (a). Note that the transmission probability is directly related to the experimentally measurable conductance.²¹ We will sketch how we have done the calculations, and we refer the readers to the literatures for more details.

In a 1D model as shown in Fig. 2 (a), the wave function on each line segment at a given positive energy E is a superposition of forward and backward traveling waves, i.e.,

$$\psi_i(x_i) = A_i e^{ikx_i} + B_i e^{-ikx_i}; \quad i = 0; 1; 2; \text{ and } 3; \quad (7)$$

where $k = \sqrt{2mE}/\hbar$ and m is the effective mass of the particle. The wavelength λ is given by $2\pi = k\lambda$. The $x_{0;1;2;3}$ are the coordinates on the line segments correspondingly, and the coordinates have positive directions as that defined in Fig. 2. We define $x_1 = x_2 = x_3 = 0$ at the right junction, and $x_0 = 0$, $x_1 = L_1$, $x_2 = L_2$ at the left junction, where $L_{1,2}$ are the lengths of the arms

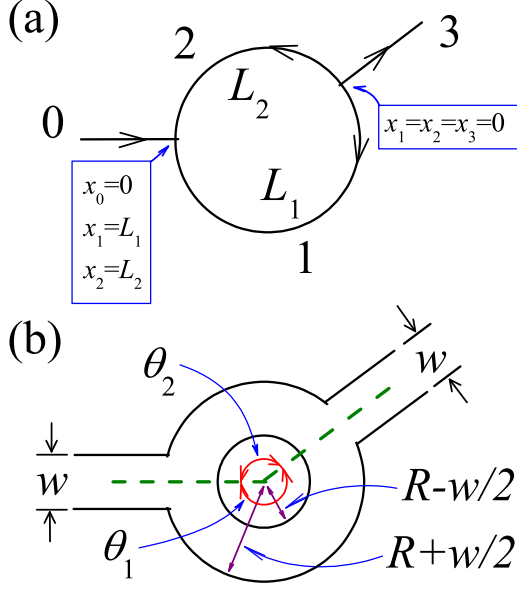


FIG. 2: (Color online) The doubly-connected 1D system and the related Q1D system we consider. (a) The 1D system is a ring (with arms labeled by 1 and 2) connected to two leads (labeled by 0 and 3). The coordinate system x_i is defined for the line segment labeled by i ($i = 0, 1, 2$, and 3). The arrows denote the positive directions of the coordinates, the right Y-junction is defined at $x_1 = x_2 = x_3 = 0$, and the left Y-junction at $x_0 = 0$, $x_1 = L_1$, and $x_2 = L_2$. (b) The Q1D system is an annulus with two radially connected leads. Both the annulus and the leads have the same width.

between the junctions [see Fig. 2 (a)]. The A_i (B_i) is the coefficient of a forward (backward) traveling wave. Since we consider particles incident from the left, we set $A_0 = 1$ and $B_3 = 0$. Then the continuity requirement

$$\psi_0|_{x_0=0} = \psi_1|_{x_1=L_1} = \psi_2|_{x_2=L_2} \quad (8)$$

and

$$\psi_1|_{x_1=0} = \psi_2|_{x_2=0} = \psi_3|_{x_3=0}; \quad (9)$$

and the Grönwall unitarity in position [following Eq. (1)]

$$\frac{\partial \psi_0}{\partial x_0} \bigg|_{x_0=0} + \frac{\partial \psi_1}{\partial x_1} \bigg|_{x_1=L_1} + \frac{\partial \psi_2}{\partial x_2} \bigg|_{x_2=L_2} = 0 \quad (10)$$

and

$$\frac{\partial \psi_1}{\partial x_1} \bigg|_{x_1=0} + \frac{\partial \psi_2}{\partial x_2} \bigg|_{x_2=0} + \frac{\partial \psi_3}{\partial x_3} \bigg|_{x_3=0} = 0 \quad (11)$$

constitute an equation set which contains six equations with the six unknowns $\{B_0; A_1; B_1; A_2; B_2; A_3\}$ which have been defined in Eq. (7). Hence the transmission amplitude A_3 can be solved, and the transmission probability $T = |A_3|^2$ be found. We may also replace the Grönwall unitarity condition by our unitarity condition [following

Eq. (6)]

$$\frac{\partial \psi_0}{\partial x_0} \bigg|_{x_0=0} + \frac{\partial \psi_1}{\partial x_1} \bigg|_{x_1=L_1} + \frac{\partial \psi_2}{\partial x_2} \bigg|_{x_2=L_2} + \frac{2}{w} \psi_0 \bigg|_{x_0=0} = 0 \quad (12)$$

and

$$\frac{\partial \psi_1}{\partial x_1} \bigg|_{x_1=0} + \frac{\partial \psi_2}{\partial x_2} \bigg|_{x_2=0} + \frac{\partial \psi_3}{\partial x_3} \bigg|_{x_3=0} + \frac{2}{w} \psi_3 \bigg|_{x_3=0} = 0 \quad (13)$$

and too the transmission probability can be solved. We will discuss the mixing of later in this paper.

Besides the mentioned 1D model, we also solve a related Q1D model in a way as that of Xia and Li in Ref. 22. Consider an annulus with an inner and an outer radii of $R - w/2$ and $R + w/2$ respectively, and two leads of width w radially connected to it as shown in Fig. 2 (b). The wave function is governed by the two-dimensional (2D) time-independent Schrödinger equation. In a lead it can be expanded in terms of transverse modes (subbands) and longitudinal forward and backward modes, i.e., $\psi_{\text{lead}}(x; y) = \sum_{l=1}^N (a_l e^{ik_l x} + b_l e^{-ik_l x}) \sin(l y w)$, where x and y are respectively the longitudinal and transverse coordinates for the lead. The k_l and l are related by $k_l^2 + (l w)^2 = 2m E / \hbar^2$, where E is the energy (positive) of the particle, and k_l can be real or imaginary. In the annulus the wave function can be expanded by radial and angular modes, i.e., $\psi_{\text{annulus}}(r; \theta) = \sum_{l=-M}^M \psi_l(r) e^{il\theta}$, where a radial mode is given by $\psi_l(r) = c_l J_l(kr) + d_l Y_l(kr)$, and $k = \sqrt{2m E} / \hbar$. The r and θ are the radial and angular coordinates respectively; and the J_l and Y_l are the Bessel functions of the first and second kinds respectively. We demand $\psi_l|_{r=R+w/2} = 0$ for any l , $\psi_{\text{annulus}}|_{r=R+w/2} = 0$ when θ is away from the leads, but $\psi_{\text{annulus}}|_{r=R+w/2} = \psi_{\text{lead}}$ when θ is in the range of a lead. Also, the radial derivative $\partial \psi_{\text{annulus}} / \partial r$ is equated with the longitudinal derivative $\partial \psi_{\text{lead}} / \partial x$ when they meet at the outer arc of the annulus. The difference between the straight transverse cuts of the leads and the outer arcs of the annulus is neglected. The wave functions in the leads and the annulus are hence matched. Expanding the wave functions in different regions with sufficient numbers of modes,²³ one gets a set of equations relating the coefficients of the modes in different regions. With a given energy E and specified in-going subbands, one can obtain the transmission probabilities in the out-going subbands.

In the Q1D case, we will consider that the particle is incident from one lead, and its energy is below the second subband and hence the particle propagates only within the first subband. The resulting transmission probability is to be compared with that in the 1D case. We will use the more convenient longitudinal wave number $k_k = \sqrt{2m(E - E_0^{\text{ann}})} / \hbar$ instead of the energy E , where E_0^{ann} is the energy of the nodeless ground state of the isolated annulus in an individual case.²⁴ Defining a longitudinal wavelength λ_k by $\lambda_k = 2\pi / k_k$ implies that the long-wavelength limit we consider is at $k_k \ll w$. Here we

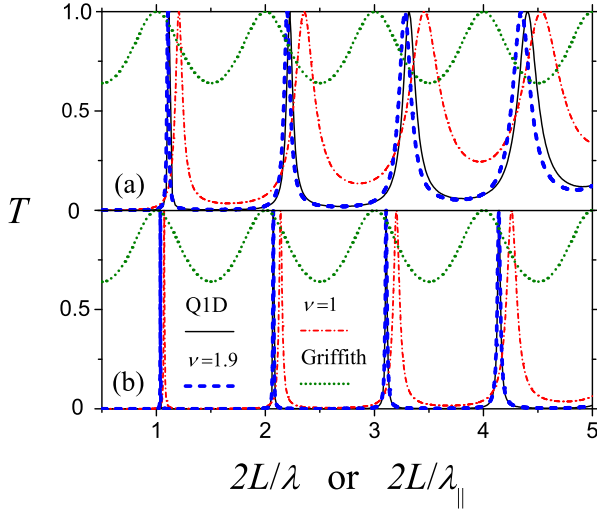


FIG. 3: (Color online) The transmission probability T is plotted versus the dimensionless longitudinal wave numbers ($2L = k$ in the case of Q1D channels, and $2L = k_{||}$ in the case of 1D channels), for the case of $L_1 = L_2 = L$. The Q1D results (solid lines), 1D results due to our scheme ($\nu = 1.9$) and dash-dotted ($\nu = 1$) lines], and 1D results due to the Griffith scheme (dotted lines) are shown. T is plotted for the cases of broad and narrow Q1D channels, (a) $R = w = 3.5$ and (b) $R = w = 9.5$. Note that the Griffith result is independent of the channel widths. In the narrow channel case [(b)], the difference between the Q1D and $\nu = 1.9$ results is indiscernible in the scale of this graph.

define the arm lengths by $L_{1/2} = R_{1/2} \sin \theta_{1/2}$, where $\theta_{1/2}$ are the angles shown in Fig. 2 (b).

III. COMPARISON BETWEEN RESULTS

Figure 3 shows the transmission probabilities obtained by different schemes, for the case of symmetrical arms in the ring ($L_1 = L_2 = L$). We have considered broad [Fig. 3 (a)] and narrow [Fig. 3 (b)] channels, and in both cases we have presented the result of the Q1D calculation, the result of the Griffith scheme, and the results of our scheme (with $\nu = 1$ and 1.9). The Griffith result is seen to differ very much from the Q1D result in all cases. The $\nu = 1$ scheme qualitatively captures the trend of change in the Q1D result when the channel width is changed, while the $\nu = 1.9$ scheme captures the Q1D result most satisfactorily.

Besides the Griffith result, it is seen that all results in Fig. 3 show Breit-Wigner (BW) resonance peaks.²⁵ These BW peaks become sharper and shift toward the left when the channels narrow down, i.e., $w = R \rightarrow 0$ [compare Figs. 3 (a) and (b)]. Those peaks are due to the quasibound levels in the arms, and they are seen to be

always blue shifted²⁶ from the exact levels. In the 1D case, the exact levels are at $2L = kL = \text{integer}$. The quasibound levels and the blue shift are results of the presence of an attractive potential at a Y-junction.²⁷ While the attractive potential in our scheme is manifest [see Eq. (6)], the potential at a Y-junction of Q1D channels is not so obvious, but can have an intuitive understanding as follows. Since a particle feels less confined at near a junction, the "band-bottom" at the vicinity of a junction is effectively lower, and therefore the region acts as an attraction center. This potential becomes stronger when the channels become narrower, and that leads to the sharper and less blue shifted BW peaks [compare Figs. 3 (a) and (b)]. The growth of the potential at narrowing channels can be understood as a result of the departure from the case of very broad channels (i.e., $w \rightarrow R$), in which the system has no difference in the "band-bottom" everywhere.

While the result from the Griffith scheme is independent of the channel width and disagrees with the Q1D result, our scheme captures the trend of change in the transmission probability when the channel width is varied. Therefore, our scheme has correctly included the attractive nature of the clean Y-junction of Q1D channels, though the strength has been underestimated (i.e., $\nu = 1.9$ is preferred to $\nu = 1$). The misjudgment of an appropriate value for the parameter ν is due to the fact that the details of the shape of the Y-junctions of Q1D channels and the actual dimensionality of the channels are relevant. For instance, our simple TB argument which leads to Eqs. (5) and (6) does not show the difference between junctions with different relative directions of branching channels, and also does not distinguish a three-dimensional (3D) cylinder from a 2D strip as a Q1D channel. But in reality, the appropriate parameter ν 's in those different cases may likely be different. In the 2D cases we have just seen in Fig. 3, the same kind of Y-junction has been involved, and the effective potential in our scheme is characterized by an almost constant ν in both the broad [Fig. 3 (a)] and narrow [Fig. 3 (b)] channel cases.

Therefore, though the parameter ν can not be derived analytically, it can be readily fixed for a particular kind of junction by comparing the 1D result with the Q1D result. What we have done in Fig. 3 has been a comparison which involves a tedious calculation. Actually, other simpler comparisons also work. For instance, one may consider the bound state at the junction due to the attraction.²⁹ On one hand, for a junction of three 1D channels, with the channels extended to infinity like what we depict in Fig. 1 (c), the negatively valued bound state energy E can be readily found by using $\psi_i = e^{-\kappa_i x_i}$, where $i = 1, 2, 3$, $\kappa_i^2 = -2mE/\hbar^2$, and Eq. (6). The energy E is found to be lower than zero by an amount of $2^{-2} \sim 2 = (9mw^2)$. On the other hand, the bound state at a T-shaped junction of three Q1D channels, with the channels extended to infinity like what we depict in Fig. 1 (a), was studied by

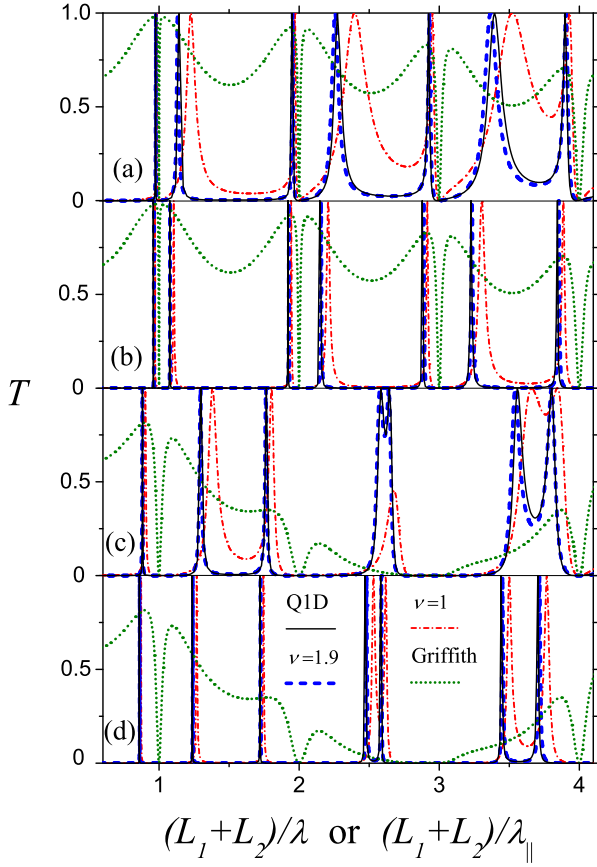


FIG. 4: (Color online) The transmission probability T is plotted versus the dimensionless longitudinal wave numbers $[(L_1 + L_2) = k$ in the case of Q1D channels, and $(L_1 + L_2) = k\lambda_{||}$ in the case of 1D channels], for the case of asymmetrical arm lengths. The Q1D results (solid lines), 1D results due to our scheme [dashed ($\nu = 1.9$) and dash-dotted ($\nu = 1$) lines], and 1D results due to the Griffith scheme (dotted lines) are shown. T is plotted for the cases of broad and narrow Q1D channels, with small and appreciable differences in the arm lengths. T is plotted for (a) $R=w = 3.5$, $L_2=L_1 = 0.9$, (b) $R=w = 9.5$, $L_2=L_1 = 0.9$, (c) $R=w = 3.5$, $L_2=L_1 = 0.7$, and (d) $R=w = 9.5$, $L_2=L_1 = 0.7$. Note that the Griffith result is independent of the channel widths. In the narrow channel cases [(b) and (d)], the differences between the Q1D and $\nu = 1.9$ results are indistinguishable in the scale of this graph.

Schult et al.²⁹ The energy of the state was numerically found to be lower than the first subband bottom by an amount of $0.19 \cdot 2\pi^2 = (2m w^2)$.²⁹ Equating the two energies in the 1D and Q1D cases, one gets $\nu \approx 2.05$, which is about the number we use in Fig. 3, and as we will see, that in Fig. 4.

Figure 4 shows the transmission probabilities for the case of asymmetrical arm lengths. It is seen that in all cases, broad channels [Figs. 4(a) and (c)] and nar-

row channels [Figs. 4(b) and (d)], small difference in arm lengths [Figs. 4(a) and (b)] and appreciable difference in arm lengths [Figs. 4(c) and (d)], there are good comparisons between the results due to our $\nu = 1.9$ scheme and the Q1D calculation. All the essential features, such as the relative positions of the BW and Fano profiles²⁸ in the Q1D results, are nicely reproduced. Note that the number 1.9 agrees with the one used in Fig. 3.

For the 1D models, including Griffith's and ours, the perfectly zero transmission dips of the Fano profiles are located exactly at the eigenenergies of an isolated ring³⁰ with a circumference of $L_1 + L_2$. In the 1D case, these eigenenergies are exactly at $(L_1 + L_2) = k(L_1 + L_2) = (2\pi) = \text{integer}$. In the Q1D cases shown in Figs. 3 and 4, the eigenenergies are numerically found to be at the $(L_1 + L_2) = k\lambda_{||}$'s deviated by not more than 0.5% from the integers on the horizontal axes. For the Q1D model, we find that those zero transmission dips may coincide with the eigenenergies of an isolated annulus only in the long-wavelength limit. As in the case of symmetrical arms, the Griffith result disagrees with the Q1D result, and our simple TB argument which leads to Eqs. (5) and (6) has underestimated the strength of the effective potential at the junction, i.e., $\nu = 1.9$ is preferred to $\nu = 1$.

IV. CONCLUDING REMARKS

It is seen that in all the above cases the results from the Griffith scheme are not in congruence with the Q1D results. The Griffith result is regardless of the channel width, whereas the Q1D result shows a strong dependence on that. Our model gives a result in much better agreement with the Q1D result. The trend of change in the transmission probability and the relative positions of the resonance profiles are impressively reproduced. In view of these calculations, it is clear that the Griffith scheme which is frequently adopted in the literature, does not describe a clean junction of Q1D channels and is definitely not for the 1D limit of the Q1D models. In the small width limit, a Y-junction of Q1D channels is a strong scatterer, and that makes the Q1D system studied in this paper not at all an "open" system. Speaking reversely, adding a repulsive potential to a Y-junction of Q1D channels may weaken the scattering effect and enhance the transmission through the junction at low energies, and away from the levels. When a strong magnetic field is present, our model may not apply since the field creates an additional asymmetrical transverse confinement.

In conclusion, we have proposed a connection scheme with a parameter ν at a Y-junction of 1D channels. The parameter ν can be most easily fixed by comparing the energy of the bound state at a Y-junction of Q1D channels, to the energy of the bound state at a Y-junction of 1D channels due to Eq. (6). The scheme reflects the presence of an effectively attractive potential at a clean

Y-junction of Q 1D channels. The disregard of this potential in the Griffith scheme makes its result compares poorly with the exact Q 1D result.

Acknowledgments – This work is supported by the

National Science Council of Taiwan under Grant No. 94-2112-M-009-017. We thank the National Center for Theoretical Sciences of Taiwan for letting us to use their facilities.

-
- * To whom correspondence should be addressed. E-mail: kkvoo@cc.nctu.edu.tw
- ¹ H. Kuhn, *Helv. Chim. Acta* 32, 2247 (1949).
 - ² J. Stanley Griffith, *Trans. Faraday Soc.* 49, 345 (1953); *ibid.*, 49, 650 (1953).
 - ³ K. Ruedenberg and C.W. Scherr, *J. Chem. Phys.* 21, 1565 (1953).
 - ⁴ T. Kottos and U. Smilansky, *Ann. of Phys.* 274, 76 (1999).
 - ⁵ B. Shapiro, *Phys. Rev. Lett.* 50, 747 (1983).
 - ⁶ M. Buttiker, Y. Imry, and M. Ya. Azbel, *Phys. Rev. A* 30, 1982 (1984).
 - ⁷ P. Exner and P. Seba, *Rep. Math. Phys.* 28, 7 (1989).
 - ⁸ Y. Gefen, Y. Imry, and M. Ya. Azbel, *Phys. Rev. Lett.* 52, 129 (1984).
 - ⁹ J.-B. Xia, *Phys. Rev. B* 45, 3593 (1992).
 - ¹⁰ J. M. Mao, Y. Huang, and J. M. Zhou, *J. Appl. Phys.* 73, 1853 (1993).
 - ¹¹ P. Singha Deo and A. M. Jayannavar, *Phys. Rev. B* 50, 11629 (1994).
 - ¹² M. V. Moskalets, *Low Temp. Phys.* 23, 824 (1997).
 - ¹³ C. M. Ryu and S. Y. Cho, *Phys. Rev. B* 58, 3572 (1998).
 - ¹⁴ C. Benjamin and A. M. Jayannavar, *Phys. Rev. B* 68, 85325 (2003).
 - ¹⁵ S. K. Joshi, D. Sahoo, and A. M. Jayannavar, *Phys. Rev. B* 64, 75320 (2001).
 - ¹⁶ B. Molnar, F. M. Peeters, P. Vasilopoulos, *Phys. Rev. B* 69, 155335 (2004).
 - ¹⁷ D. Bercioux, M. G. Overmire, V. Cataudella, and V. M. Ramaglia, *Phys. Rev. Lett.* 93, 56802 (2004).
 - ¹⁸ P. Földi, B. Molnar, M. G. Benedict, and F. M. Peeters, *Phys. Rev. B* 71, 33309 (2005).
 - ¹⁹ U. Aebi, K. Wakabayashi, and M. Sigrist, *Phys. Rev. B* 72, 75328 (2005).
 - ²⁰ Note that the information of the relative directions of the branches is not contained at this level. This information will be included later via a phenomenological parameter in Eq. (6).
 - ²¹ S. Datta, *Electronic Transport in Mesoscopic Systems* (1st edition), Cambridge University Press (1995).
 - ²² J.-B. Xia and S.-S. Li, *Phys. Rev. B* 66, 35311 (2002).
 - ²³ The Q 1D results in Figs. 3 and 4 are obtained using 101 transverse modes in the leads (i.e., $N = 101$) and 101 angular modes in the annulus (i.e., $M = 50$). The differences between these results and that using $N = 201$ and $M = 100$ are well within the thicknesses of the data lines in the figures.
 - ²⁴ E_0^{ann} is slightly lower than the energy of the band-bottom of the 1st subband in the leads, $\tilde{\omega}^2 = (2m\omega^2)$.
 - ²⁵ G. Breit and E. Wigner, *Phys. Rev.* 49, 519 (1936).
 - ²⁶ We mean a red (blue) shift of a quasibound level by a shift of the level to an energy lower (higher) than the level at the infinite trapping potential limit, where the wave function is expelled completely from the barriers or antibarriers.
 - ²⁷ Recall the fact that a quasibound level due to repulsive barriers (attractive wells) is red (blue) shifted.
 - ²⁸ U. Fano, *Phys. Rev.* 124, 1866 (1961).
 - ²⁹ R. L. Schult, D. G. Ravenhall, and H. W. W. Yld, *Phys. Rev. B* 39, 5476 (1989).
 - ³⁰ K.-K. Voo and C.-S. Chu, *Phys. Rev. B* 72, 165307 (2005).